Edge Directed Radial Basis Function based Interpolation Towards PCA based PAN-sharpening

Ramen Pal, Hasina Begum, Somnath Mukhopadhyay, Sunita Sarkar, Debasish Chakraborty, Sumit Majumdar & Diganta Sengupta

Published online: 25 Oct 2021.

Submit your article to this journal ⟗

Article views: 20

View related articles ⟗

View Crossmark data ⟗

Taylor & Francis
Taylor & Francis Group

Check for updates

Edge Directed Radial Basis Function based Interpolation Towards PCA based PAN-sharpening

Ramen Pal[a], Hasina Begum[a], Somnath Mukhopadhyay [a], Sunita Sarkar[a], Debasish Chakraborty[b], Sumit Majumdar[c] and Diganta Sengupta[d]

[a]Department of Computer Science and Engineering, Assam University, Silchar, India; [b]RRSC-East, Indian Space Research Organization, Kolkata, India; [c]Department of Computer Science and Engineering, MCKV Institute of Engineering, Howrah, India; [d]Department of Computer Science & Engineering, Meghnad Saha Institute of Technology, Kolkata, India

ABSTRACT

In this research, we proposed a new PAN-sharpening algorithm by using edge-directed Gaussian Radial Basis Function (RBF) and Principal Component Analysis (PCA). Up-scaling is a procedure to upgrade the spectral data of a Low Resolution (LR) Multi Spectral (MS) imagery. Non-linear up-scaling methods generate fewer artefacts in the interpolated image as they are edge-adaptive in nature. Adaptive interpolation techniques consider different features of an image during up-scaling. These techniques are proven efficient compared with non-adaptive methods. However, they may generate distorted output in fine-textured areas and can have lower luminance information. We consider the Laplacian of Gaussian (LoG) or Marr-Hildreth edge detection operator to preserve missing structure and luminance information. It generates smooth edges by minimizing artefacts in the interpolated image. We have considered multi-source and multi-sensor datasets obtained from LISS-IV, CATROSAT-I, and Quickbird to perform all experiments. We have carried out a broad quantitative and subjective assessment and comparison of the proposed algorithm with the standard and cutting-edge methods.

1. Introduction

The study of the Earth's natural features, remote object identification, climate, weather study, the study of the exterior and interior structure of Earth, hydrology, soil erosion, forestation, and different fields of agriculture, and surveillance widely use Satellite images Daamouche and Melgani (2009). It is necessary to execute a sequence of preprocessing and fundamental corrections on the remote sensing images before performing Land-use /Land-cover (LULC) segmentation or classification (Bruzzone et al. (2006), Venkatakrishnamoorthy and Reddy (2019)). In a satellite image, spatial resolution alludes to the smallest component of the surface detected by a sensor. The spectral resolution of an image gives the wavelength intervals of different elements in the image. An image with a higher spectral resolution can distinguish the elements more efficiently. In contrast,

---

an image with higher spatial resolution can detect smaller features. PAN image has a high spatial resolution and low spectral resolution Pohl and van Genderen (1998). At the same time, the MS image has low spatial resolution and high spectral resolution. The fusion of PAN and low resolution-MS (LR-MS) images generates a high-resolution MS (HR-MS) image Zhang et al. (2019), and the process is known as the pan-sharpening Li et al. (2018). It preserves the MS image's spectral property, and spatial property of the PAN image Chavez Jr. et al. (1991).

The pan-sharpening algorithm's primary condition is that the PAN image and the LR-MS image should be co-registered and geo-referenced by Pohl and van Genderen (1998). Nowadays, both the PAN and MS sensors are mounted on the same platform. It eliminates the general problem of co-registration by simultaneously acquiring images. Modern commercial satellites like IKONOS, Quickbird, SPOT, WorldView, Geo-eye, etc., can produce PAN images with a spatial resolution of below half a metre, and MS images can have up to eight spectral bands.

In image processing, resolution enhancement of the MS image is a need for several applications. This is done by image up-scaling. This procedure increases the pixel data in an image and estimates the new pixels' intensity value, based on the existing pixel values. The estimation of new pixel values is called image interpolation Huang and Liu (2020). The fusion is then done by embedding the intensity information of the PAN image into the interpolated MS image. In the literature, several interpolation techniques are reported. Among them, Nearest-neighbour, Bi-linear, Bi-cubic, Wavelet, and Radial Basis Function (RBF)-based interpolation techniques are proven to be efficient with respect to any of the following reasons: i) ease in the implementation, ii) quality of the outcome, iii) execution time Ablin, Sulochana, and Prabin (2019), Azam, Zohra, and Islam (2014). Several fusion techniques are also reported in the literature. Among them, Hue Intensity Saturation (HSI) Choi (2006), Principal Component Analysis (PCA) Shahdoosti and Ghassemian (2016), General Intensity-Hue-Saturation (GIHS) Zhou et al. (2014) based image fusion techniques are popular. These approaches mainly suffer from one or more of the following short-comings: i) Degradation of spectral information in the fused image, ii) Poor spatial resolution, iii) Application dependent, iv) Computational complexity is high.

In this research, we propose a new edge-directed RBF-based interpolation and PCA-based image fusion technique that is free from all the shortcomings as mentioned above. We perform an extensive experimental study to compare the proposed method's performance by using different combinations of PCA, HIS, Nearest-neighbour, Bi-linear, Bi-cubic, and Wavelet-based methods. We also validated our method with the seven state-of-the-art methods. We considered the dataset obtained from CATROSAT-1, LISS-IV, and QUICKBIRD satellite sensors for the experiment. A detailed survey of the related works is presented in Section 2.

2. Related works

Interpolation plays a key role in increasing the efficiency of image fusion Demirel and Anbarjafari (2011). It is the procedure of calculating or approximating a new pixel's intensity value, depending on the value of a region's known pixel intensity values. In general these methods can be categorized in two groups: i) non adaptive, and ii) adaptive. In Non adaptive methods all pixels has equal contribution towards the interpolation. It

only uses neighbouring pixels value to predict the value for the missing pixels. Whereas, adaptive interpolation technique uses spatial as well as spectral features towards predicting the value of missing pixels. We can observe from the literature that in last few decades non-adaptive methods such as Nearest Neighbour Angelos and Ioannis (2009), Bi-linear Dahiya, Garg, and Jat (2013), Bi- cubic Hwang and Lee (2004), Lanczos Madhukar and Narendra (2013), Inverse Dis- tance Weighted Arun (2013), Interpolation with Unsharp Masking Teoh, Ibrahim, and Bejo (2008), Discrete Wavelet Transform etc. are extensively used in remote sensing related applications. The nearest neighbour up-scaling method finds the closest corresponding pixel in the original image and approximates each pixel's value in the output image. Due to this simplistic nature, it suffers from artefacts (blurring, ringing) Karimi, Kangarloo, and Javadi (2014). Bilinear up-scaling takes a weighted mean of the four (2×2) neighbouring pixels to estimate its interpolated pixel value in the output image. This technique interpolates in two directions (horizontal and vertical). It can generate some visible artefacts and blurring effects in the up-scaled image Singh and Goyal (2015). The bicubic interpolation method considers the closest 16 pixels, i.e. 4×4 neighbourhood of the known pixels. These pixels are distributed at various distances from the unknown pixel. The pixels are assigned with varying weights in the calculation. Computational cost and output quality of this method are reasonable Shreyas (2014). Lanczos interpolation is done based on a separable filter called Lanczos filter. This filter is sinc function based three lobed window. In this technique, first an image is divided into unique samples and then each sample is mapped to an interpolated window. This is achieved by using the reconstruction or Lanczos kernel. This kernel can assume negative values. So, during interpolation it can generate negative values. Thus a rescaling procedure is used here to scale all values in the interpolated window within the range of input values Moraes et al. (2020). Inverse distance weighted interpolation technique is inspired by the Tobler's first law of Geography. It is a multivariate interpolation technique. It approximates the value for the missing pixels by calculating weighted average of its closest pixel values. This technique generates degraded output if the intensity values of the input image is unevenly distributed Ozelkan et al. (2015). Unsharp Masking (UM) generates a sharpened image by subtracting the image with the blurred version of it. In this technique a linear (For example Bi-linear) or area interpolation technique (For example Lanczos-3) is required to up-scale the image in different stages Acharya and Meher (2012). Discrete Wavelet Transform (DWT) converts an image into discrete samples. Samples are the approximate, horizontal, vertical, and diagonal details of the original image Temizel (2007). It is done by using Multi-Resolution Analysis (MRA). Three subbands, low-high (LH), high-low (HL), and high-high (HH), contain the high-recurrence parts of the MS input image. We can get the inexact (LL) coefficients by filtering MS image with a low-pass channel. Therefore, instead of using less informative LL, we can use the LR-MS image for interpolation. Supplanting the LL sub-band with the MS image improve the standard of the objective scaled image. The interpolation factor (a), of the input LR-MS image is half of the high-frequency sub-bands' interpolation factor. After interpolating the input LR-MS image by $\frac{a}{2}$ and interpolating LH, HL, and HH by a, and then applying Inverse DWT (IDWT), the output image is generated. The output MS image contains sharper edges than the input MS image. All these non adaptive methods can produce degraded outputs because of their inability to enhance the edges and high frequency information properly.

Thus interpolated image can contain artefacts like blurring, aliasing. Adaptive methods can minimize these shortcomings by considering edge information during interpolation. These edge directed interpolation techniques adapts the structure across the edges by applying different operators and refine it. In this technique a blurred image is generated by using Soft decision based adaptive interpolation technique of Zhang et al. Zhang and Xiaolin (2008) uses multiple autoregressive model for different features of an image. Then it calculates the value for the missing pixels by using a soft decision estimation technique. It has a mismatch problem of geometric duality during the estimation of parameters. This issue is resolved by Li et al. Hung and Siui (2012). It employs a weighted-least-square-estimation model to estimate parameter as well as data. Adaptive interpolation method of Li and Orchard (2001) estimates the missing pixel value by using the geometric duality between the co-variances of high resolution and low resolution images. Polsel et al. proposed Ji, Zhong, and Ma (2020) proposed a multi-scale deep learning based adaptive image interpolation method. It considered attention-aware inception network. This network works in two stages. In the first stage features from low-resolution image are extracted. In the second stage interpolation is done by mapping these features to the image. This is an efficient model, but the complexity of this model is high. So it's not suitable in real time applications.

Image fusion can be performed by using pixel or feature or decision level Kaur and Neeru (2017). At the pixel level, fusion is performed utilizing low-level data from the image in the spatial or transform space. In the feature level, an image is divided into equal-length small areas. Then fusion is done by using properties and information from adjacent small areas. Whereas in decision level, fusion is done by using the properties of different classes obtained by segmenting or classifying the input image. Among them, pixel-level image fusion techniques are efficient due to its capability of detecting noises, enhance pixel-level features, and less complex in nature Pohl and van Genderen (1998), Shreyas (2014). Fusion techniques such as Brovey transformation (BT), HIS Transformation, PCA-based techniques, Wavelet transformation, and Gram-Schmidt (GS) method are works at the pixel level. Each fusion method gives a different colour effect in the fused image. PAN-sharpening algorithms are classified into two categories, i.e. component substitution (CS) based methods and multi-resolution analysis-based method (MRA) Baronti et al. (2011). BT, HIS, PCA, and GS method falls under the category of CS-based methods. Whereas the high pass filter method, the wavelet-based fusion method falls under the MRA method Meng et al. (2019). In the CS-based method, the first MS bands are projected to a new domain. Then, one of the new domain components depending on the spatial information is replaced by PAN image Meng et al. (2019). In MRA based fusion, the MS image is decomposed into several bandpass channels. Then high-frequency channels of the PAN image are injected into the corresponding channel of the MS image Aiazzi et al. (2009), Meng et al. (2019). In the Brovey transform, method Pohl and van Genderen (1998), each band of the MS image was divided by the summation of all bands. Then, newly computed values are element-wise multiplied with the PAN image to get the fused image. It is one of the SC-based approach Panchal and Thakker (2015). However, this method suffers from high colour distortion. In the HIS transformation method, Red, Green, and blue bands of the MS image are converted into Hue, Saturation, and Intensity bands. Then the intensity ban is to replace the pan-chromatic band. The HIS transformation Carper, Lillesand, and Kiefer

(1990), Chavez, Sides, and Anderson (1990), Gowri et al. (2015), Pohl and van Genderen (1998), based fusion technique is a CS-based pan-sharpening method Panchal and Thakker (2015). HIS transformation technique suffers from high spectral distortion due to the large radiometric difference between the intensity, and panchromatic band Gowri et al. (2015). In PCA based fusion method Chavez and Kwarteng (1989), Chavez, Sides, and Anderson (1990), Panchal and Thakker (2015), the first Principal Component (PC1) of the LR-MS image is substitute with the histogram matched PAN image. The relationship between original and fused images can be derived by using statistical methods Panchal and Thakker (2015). In the Gram-Schmidt fusion method Cunjun et al. (2004); Laben and Brower, the LR-MS image is converted into a low-resolution PAN image (LR-PAN) by taking an average of all the bands. Then considering the generated LR-PAN image as the first band, the Gram-Schmidt (GS) transformation Cunjun et al. (2004) of the LR-PAN, and the LR-MS image is executed. In the next step, necessary adjustments were made to the high-resolution PAN image, and then it substitutes the first band of the GS transformed image. Finally, by performing the inverse GS transformation, the fused image had been generated. It performs better for maximization image sharpness and minimizing colour distortions Wang et al. (2005). The aforementioned methods mainly suffer from one or both of the following shortcomings: i) spectral distortion, ii) inability to achieve high spatial resolution Amro et al. (2011). In Shen et al. (2019a), a hybrid method of pan-sharpening is discussed. This algorithm acquires the gradient of the HR-MS image by using a variational model. Then it is used in constructing a convolution neural network-based fusion model.

3. Motivation and contributions

The quality of pan-sharpening depends on the underlying interpolation technique. Linear upscaling methods lead to artefacts. However, non-linear upscaling methods can reduce these shortcomings as they are edge adaptive in nature. In Section 2, we discussed that adaptive interpolation technique considers image features for performing interpolation. So, it can generate efficient outcomes compared to the non-adaptive algorithms. However, it may also generate degraded output in fine-textured areas of the image. This shortcoming can be minimized by taking the benefit of a second-order differentiation-based edge detection operator (for example, Laplacian, Marr-Hildreth edge detection operator, etc.). These methods are isotropic in nature. Like humans, it can detect edges in all directions within a kernel. It can preserve missing structures and luminous information by maintaining the spatial property of the image. These informations can be used at different stages to minimize the distortion of the interpolated image. Based on the above discussion, we can summarize that a pan-sharpening method should:

  (i) be capable of generating solution with low spectral distortion and high spatial resolution,
 (ii) be able to reduce artefacts,
(iii) have less computational overhead.

In this research, we propose a mixture approach of fusion by considering these requirements. The contribution of our research is as follows:

(i) Minimizing spectral distortion by using a new adaptive approach of edge directed RBF-based non-linear interpolation algorithm. It also reduces artefacts across the edges.
(ii) Incorporating the second-order derivative-based Laplacian of Gaussian (LoG) or Marr-Hildreth edge detection operator to improve the quality of the interpolated image.
(iii) Maximizing the spatial resolution by efficiently fusing upscaled and panchromatic images using PCA.
(iv) Extensive comparative assessment of the results of different interpolation techniques with respect to PCA and HIS-based fusion.

The remaining parts of the paper are coordinated as follows: The proposed algorithm is discussed in Section 4. Results are examined in Section 5. The conclusion is attracted in Section 6.

4. Proposed algorithm for image fusion

The proposed PAN-sharpening algorithm is graphically presented in Figure 1. In this method, the first image interpolation is performed on the MS image by using the edge directed RBF-based upscaling method. It is discussed in Subsection 4.1. Then, PCA-based image fusion is performed on upscaled and VHR PAN image by using the PCA-based PAN-sharpening algorithm. It is discussed in Subsection 4.2.
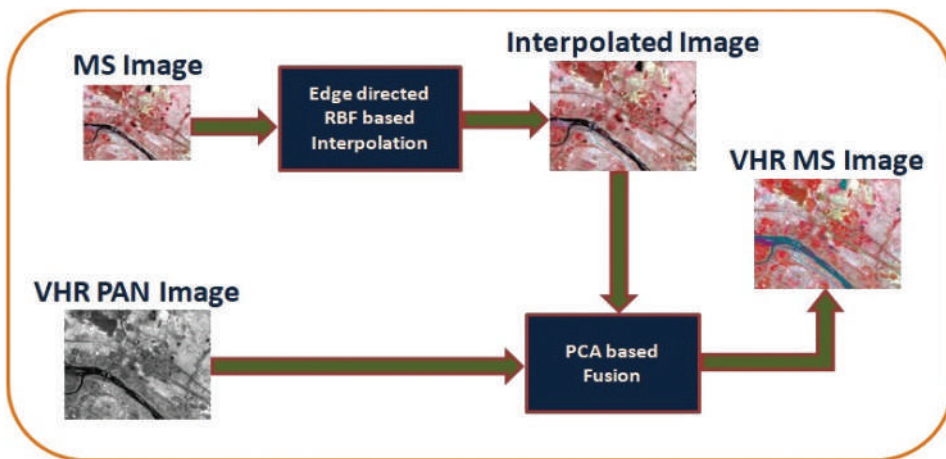

Figure 1. Proposed PAN-sharpening algorithm.

4.1. Edge directed RBF based interpolation

If a function only depends on its input argument's magnitude, then it is treated as a Radial Basis Function (RBF) Muzhou and Xuli (2011). It is used to estimate any multivariate disperse dataset Bureerat and Pholdee (2018). It has a distance function that calculates every pixel's distance with its adjacent data points and places that pixel in a position in an unrestricted manner. RBF is used to interpolate images due to the property, as mentioned above.

Our goal is to develop a system with less computational overhead and higher efficiency. Among several available radial functions, the Gaussian radial function has very little computational overhead and is as simple as a linear method. However, this function generates artefacts like ringing or staircase curves across the edges in the upscaled image Gao et al. (2019). Edge-directed Gaussian function efficiently overcomes these shortcomings. So, we considered edge-directed Gaussian radial function Han et al. (2016), Wang, Shi, and Atkinson (2014a) for performing the interpolation. The proposed method for image interpolation is presented in Figure 2. In this technique, the input MS image (X) with size $M \times N$ pixels is first enlarged to an image (Y) in both horizontal ($M \times \lambda$) and vertical ($N \times \lambda$) direction by using Equation (1).

$$Y = \begin{bmatrix} \lambda & 0 \\ 0 & \lambda \end{bmatrix} \times \begin{bmatrix} S_m \\ T_n \end{bmatrix} \qquad (1)$$

Here, an element in coordinate S and T of X is interpolated by an interpolation factor (λ) in horizontal and vertical directions. It (λ) is the proportion of spatial resolution among input PAN and MS images. We find that interpolation depends on zero stuffing Pflugfelder and Scharr (2020). Thus, λ should always be an integer value. For some sets of MS and PAN images, it is possible to get a fractional value for λ. In these cases, we have considered resampling Kim, Kim, and Park (2020) to achieve the overall fractional factor. It is a combination of interpolation and decimation operations. For example, if for a set of input image we get $\lambda = \frac{5}{2}$, then the MS image is first interpolated by $\lambda = 5$, after that it
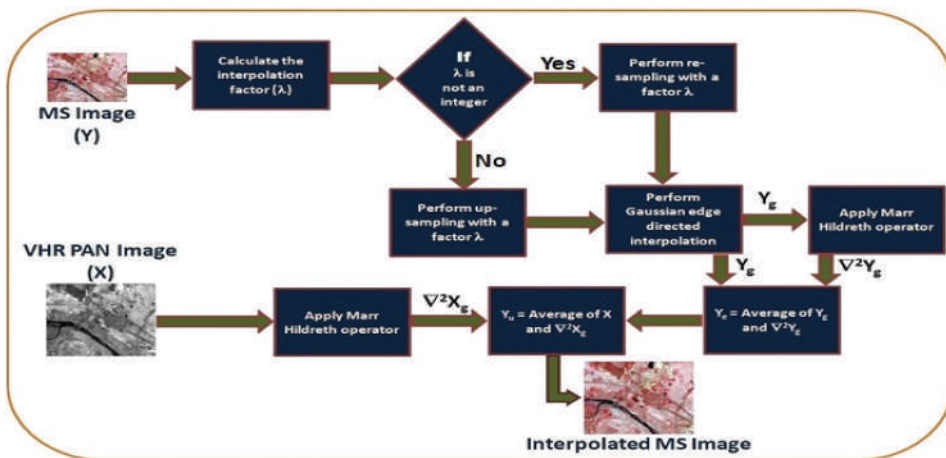

Figure 2. Proposed method for edge-directed RBF based interpolation.

decimated by $\lambda = 2$. Y contains indeterminate pixels as these are interpolated by using the determinate pixel values of X. Therefore, in the next step, acceptable values ($Y_g(r, s)$) for these indeterminate pixels are calculated by using Equation (2).

$$Y_g(r, s) = \sum_{i=0}^{u} \sum_{j=0}^{v} Y(r+i, s+j)\phi_g(i, j) \tag{2}$$

The value of i and j should be in the range 1 to $M \times \lambda$ and 1 to $N \times \lambda$ respectively. It is done by convolving Y with a Gaussian kernel $\phi_g(u, v)$ of size $u \times v$. The kernel is presented in Equation (3).

$$\phi(u, v) = \frac{1}{\sigma\sqrt{2\pi}} \times e^{\frac{-ed^2}{2dg}} \tag{3}$$

Here, d_g is the degree of regularity or smoothness of ϕ_g and σ is the standard deviation. ed is the euclidean distance between the centre pixel and the other pixels in the kernel of size $u \times v$. It is calculated by using the distance function presented in Mukhopadhyay et al. (2020). After that, a second-order derivative-based isotropic Laplacian of Gaussian (LoG) or Marr-Hildreth operator Guo et al. (2018) is applied on the Y_g to enhance its quality. It preserves the luminous intensity information of an input image across all possible directions of the mask. So, it can detect edges in any direction. It is a linear blend of different partial derivatives. It is presented in Equation (4).

$$^2Y_g(u, v) = \left\{ \frac{\partial Y(u)}{\partial u^2} \times Y(v) \right\} + \left\{ \frac{\partial Y(v)}{\partial v^2} \times Y(u) \right\} \tag{4}$$

We can observe that ^2Y_g contains the smooth edge information of Y_g. As a result, an enhanced MS image (Y_e) is generated by calculating the mean of ^2Y_g and Y_g. We know that HR PAN image (X) contains more detailed information about the edges. It can also enhance the quality of the Y_e. So, the edge information (^2X_g) of X is also extracted by using Equation (4). Finally, the interpolated image (Y_u) is obtained by calculating the mean of each band of Y_e and X_e.

4.2. PCA based PAN-sharpening

In PCA (Principal Component Analysis), new variables or Principal Components (PCs) are calculated using the relation between variables of the original dataset. These are linear functions with respect to the original variables and are uncorrelated with each other Ooi et al. (2016). We have considered PCA to perform the upscaled and PAN image fusion for the above-mentioned reasons. It is presented graphically in Figure 3.

We find that all bands in an MS image are correlated in nature. Hence, the PAN image cannot be replaced with any band. So, we have applied PCA to convert the correlated bands of the upscaled MS image (Y_u) into non-correlated PCs. In this algorithm, first, each band from the Y_u is reshaped into a one-dimensional matrix (C). Then, the mean adjusted matrix (C_M) is calculated from each C. After that, the covariance matrix ($covS$) of C_M is calculated. Then, the eigenvalues (E_{val}) and vectors (E_{vec}) are calculated for each coV. All the E_{vec} are arranged in decreasing order based on their E_{val}. Then PCs are calculated by multiplying C_M with E_{vec}. PCs are the linear functions of all bands in Y_u. The first principal
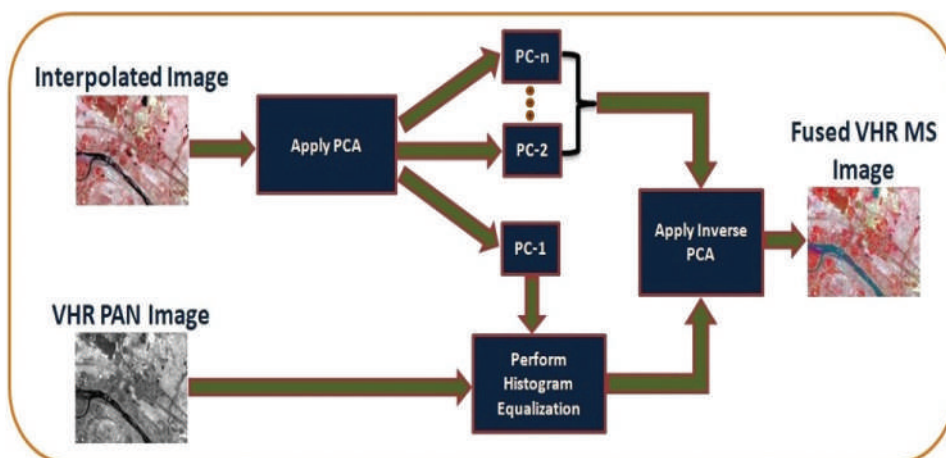
Figure 3. Proposed method for PCA based PAN-sharpening.

component or $PC - 1$ contains the maximum spatial information about Y_u with the highest variance, whereas P contains higher spatial information because of it's spatial resolution. So, we can embed P in place of $PC - 1$. In this operation, first, the histogram of P is matched with $PC - 1$. Then, the $PC - 1$ is supplanted by the P. Finally, inverse PCA is executed on PCs to generate the Very High Resolution (VHR) fused image.

5. Results and discussion

In this section, we have presented the full analysis of the proposed method and comparison with the standard and state-of-the-art methods. We have implemented and tested the proposed method in a system with the following set up:

(1) Editor: Spyder (Anaconda-3)
(2) Coding Language: Python 3.9.0
(3) Operating System: Windows (Version: 10)
(4) RAM: 16 GB
(5) Processor: Intel(R)-$Core^{TM}$-i5-L16G7-3.0 GHz.

5.1. Quantitative assessment functions

We have considered six distinctive image quality parameters, i.e., Correlation Coefficient (*CC*), Root Mean Square Error (*RMSE*), Peak Signal-to-Noise Ratio (*PSNR*), relative dimensionless global error (*ERGAS*), Universal Image Quality Index (*UIQI*) and Structural Similarity Index Measure (*SSIM*) to quantify the quality of the interpolated and PAN-sharpened images. These functions require two images that are of size as input. So, the fused image is re-sampled (by using our proposed method) to the length of the input MS

image for evaluating these functions. The input MS image is utilized as the reference image. The correlation coefficient shows the level of relationship between the refereed (MS) and fused images. It is introduced in Equation (5).

$$CC = \frac{\sum_i (r_i - r_m)(f_i - f_m)}{\sqrt{\sum_i (r_i - r_m)^2 (f_i - f_m)^2}} \tag{5}$$

Here, r_i and f_i are the intensity information of ith pixel in the refereed (R) and PAN-sharpened image (F) respectively. r_m and f_m are the mean intensity values of the referenced and fused images, respectively. The RMSE is the measure of validating the fused image against the reference image Dennison and Roberts (2003). It is presented in Equation (6).

$$RMSE = \sqrt{\frac{\sum_{i,j=1}^{mn} (R_{ij} - F_{ij})^2}{mn}} \tag{6}$$

Here, R_{ij} and F_{ij} are the intensity information of the $(i,j)^{th}$ pixel of the R and F, respectively. m and n defines the total number of rows and columns of F. The lower value of RMSE is better. Ideally, it should be 0. The PSNR is the proportion between the most extreme conceivable intensity value of an image and the intensity of the debasing noise Huynh-Thu and Ghanbari (2008). It is calculated by using Equation (7).

$$PSNR = 10 \times log_{10} \left(\frac{P^2}{\frac{\sum_{i,j=1}^{mn} (R_{ij} - F_{ij})^2}{mn}} \right) \tag{7}$$

Here, P is equal to $(2^b) - 1$, where b is the absolute number of bits utilized to represent a pixel of the R. Higher value of PSNR is better. ERGAR is a popular global quantitative image quality index for PAN-sharpening Du et al. (2007). ERGAS indicates the volume of spectral deformation in the PAN-sharpened image. It is evaluated by using Equation (8).

$$ERGAS = 100 \times \frac{hr}{lr} \sqrt{\frac{1}{N} \Sigma_{i=1}^{N} \left(\frac{RMSE_i}{\mu_i} \right)^2} \tag{8}$$

Here, hr and lr are the spatial resolution of the input PAN and MS images individually. N defines the total number of bands presents in the input MS image. $RMSE_i$ represents the RMSE and μ_i represents the mean of ith spectral band of the PAN-sharpened image. Since the ERGAS value is dependent on the RMSE, the lower value of ERGAS indicates the better quality of the fused image. UIQI mainly takes CC, luminance distance, and contrast distortion of the R and F into consideration Wang and Bovik (2002). The UIQI of R and F is calculated by using Equation (9).

$$UIQI(R, F) = \frac{\sigma_{RF}}{\sigma_R \sigma_F} * \frac{2\mu_R \mu_F}{\mu_R^2 + \mu_F^2} * \frac{2\sigma_R \sigma_F}{\sigma_R^2 + \sigma_F^2} \tag{9}$$

Here, μ_R and μ_F are the mean of R and F, respectively. σ_R and σ_F defines the standard deviation of R and F, respectively. σ_R^2 and σ_F^2 are the variance of R and F, respectively. σ_{RF} is the covariance of R and F.

The *SSIM* is an improvement over *UIQI* Wang et al. ([2004](#)). It quantifies the similarity between intensity in the local pattern of *R* and *F*. It varies within $-1 \, to + 1$. *SSIM* equals to $+1$ indicates that the referred and the fused images are the same. So, the higher the value of SSIM, the better. It is calculated by using Equation (10).

$$SSIM(R, F) = \left(\frac{2\mu_R\mu_F + C_1}{\mu_R^2 + \mu_F^2 + C_1} \right) \left(\frac{2\sigma_{RF} + C_2}{\sigma_R^2 + \sigma_F^2 + C_2} \right) \tag{10}$$

Here, K_1 and K_2 are two constants. L defines the maximum intensity value and C_1, C_2 are two constants given by $(K_1 L)^2$ and $(K_2 L)^2$ respectively.

5.2. Quantitative and qualitative evaluation and validation

We have discussed all the experimental results in two phases. In the first phase, a comparison between the standard and three state-of-the-art methods is discussed by using a multi-source VHR dataset. Whereas in the second, we have tested the performance of the proposed algorithm with eight different cutting-edge methods by using another multi-sensor VHR dataset. All the images are radiometrically corrected and geo-referenced. The first VHR dataset is comprised of the VHR PAN image is taken from CARTOSAT-1 and MS image is taken from LISS-IV satellite sensors. PAN image has 2.5-metre spatial resolution and contains a 1478 × 1898 number of pixels. The MS image contains the following three bands: i) non-infrared (NIR), ii) green and iii) blue. It has a 6-metre spatial resolution and comprises 607 × 841 number of pixels.

The proposed method for image fusion is applied on this dataset. λ is calculated as 6/2.5, based on the spatial resolution of the input PAN and MS images. It is normalized as $\lambda = 12/5$. λ is a fractional value. So, re-sampling is applied to enlarge the MS image. Here the image is first up-sampled with $\lambda = 12$. Then, the outcome is decimated with $\lambda = 5$. Then, it is interpolated by using the proposed interpolation technique. We have implemented and executed standard interpolation techniques such as the nearest neighbour, bi-linear, bi-cubic, wavelet, Gaussian RBF, and cutting-edge methods like Wang, Shi, and Atkinson ([2014b](#)), Casciola et al. Casciola and Morigi ([2010](#)), Lee and Yoon ([2010](#)) on the dataset. Interpolated images obtained by using these methods and the proposed method are presented in [Figure 4](#). The effect of the different interpolation methods on the marked part of the input MS image is shown in this figure. We can observe from the three different marked portions on these images that our proposed method can preserve better edge information compared to others. It can generate a more sharpened interpolated MS image. Our method holds spectral information better than the other methods.

Then, the proposed PCA-based PAN-sharpening algorithm is used to generate the PAN-sharpened image by using the up-scaled image generated by using the proposed interpolation algorithm and the PAN image from Dataset-1. PCA and HIS based image fusion techniques are also applied on the interpolated image obtained from the standard interpolation methods. We have also applied PCA-based fusion technique on the up-scaled images generated by the cutting-edge methods and the general Gaussian RBF method. Fused images generated by using these methods are presented in [Figure 5](#). The effect of the different methods on the marked part of the input MS and PAN image are shown in this
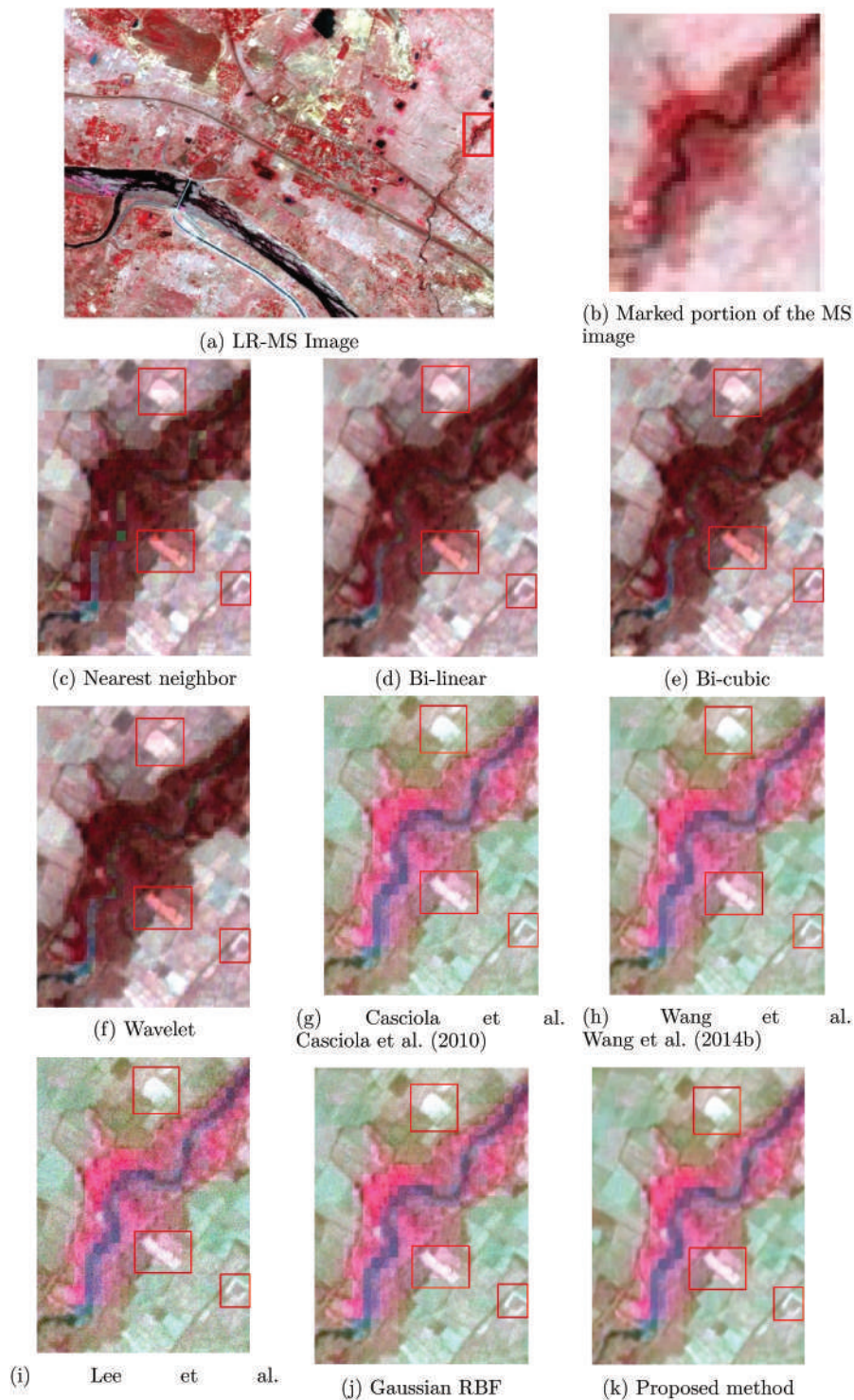
Figure 4. Qualitative validation of the proposed method for the MS image from the Dataset-1: (b) Marked part of the LR-MS image, and after interpolation using: (c) Nearest neighbour, (d) Bi-linear, (e) Bi-cubic, (f) Wavelet, (g) Casciola et al. Casciola and Morigi (2010), (h) Wang et al. Wang, Shi, and Atkinson (2014b), (i) Lee et al. Lee and Yoon (2010), (j) Gaussian RBF, and (h) Proposed method.
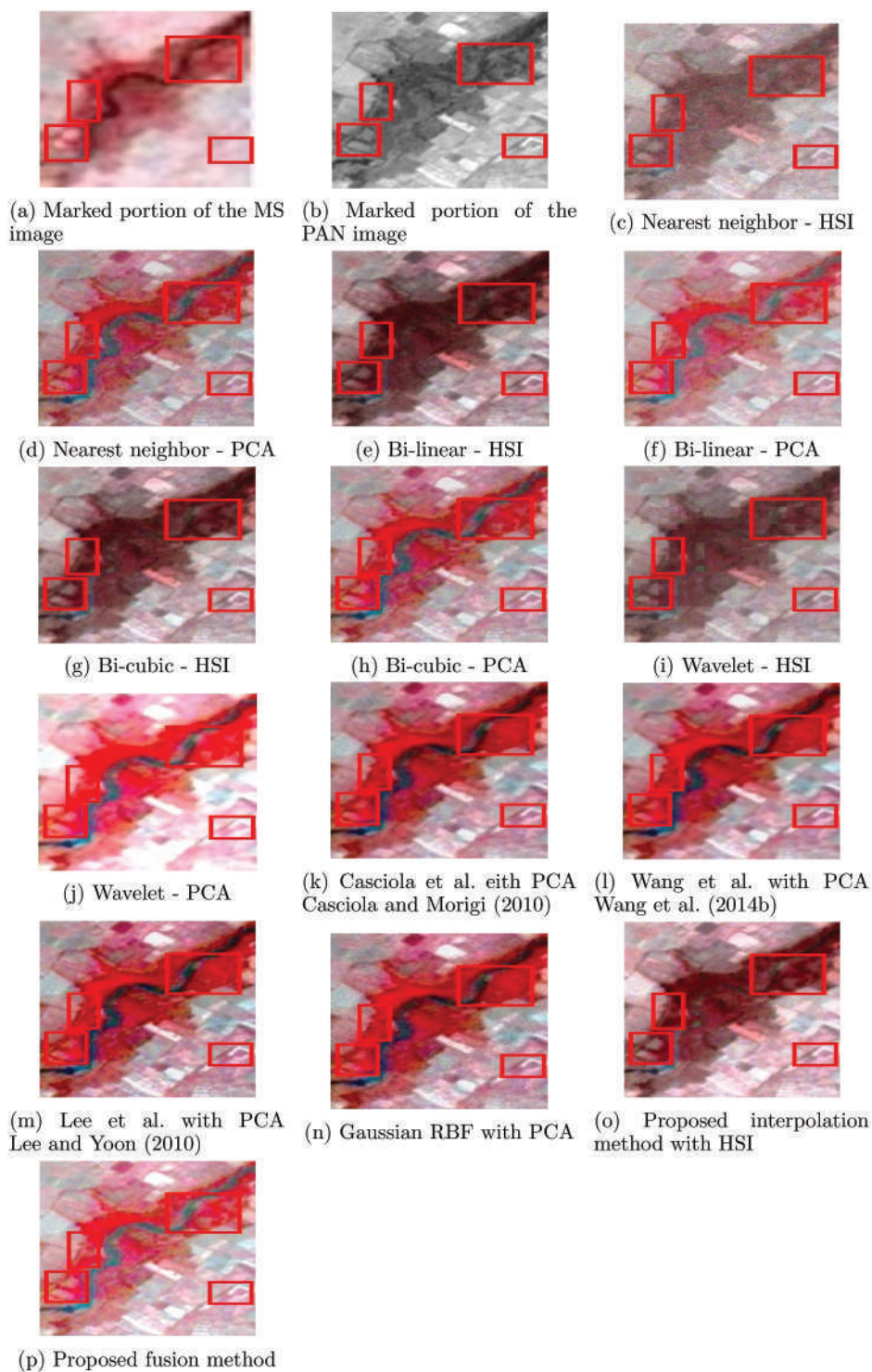
(a) Marked portion of the MS image
(b) Marked portion of the PAN image
(c) Nearest neighbor - HSI
(d) Nearest neighbor - PCA
(e) Bi-linear - HSI
(f) Bi-linear - PCA
(g) Bi-cubic - HSI
(h) Bi-cubic - PCA
(i) Wavelet - HSI
(j) Wavelet - PCA
(k) Casciola et al. eith PCA Casciola and Morigi (2010)
(l) Wang et al. with PCA Wang et al. (2014b)
(m) Lee et al. with PCA Lee and Yoon (2010)
(n) Gaussian RBF with PCA
(o) Proposed interpolation method with HSI
(p) Proposed fusion method

Figure 5. PAN-sharpened images obtained for the first dataset by using: (a) Marked portion of the MS image, (b) Marked portion of the PAN image, (c) Nearest neighbour and HIS based fusion, (d) Nearest neighbour and PCA based fusion, (e) Bi-linear and HIS based fusion, (f) Bi-linear and PCA based fusion,

(g) Bi-cubic and HIS based fusion, (h) Bi-cubic and PCA based fusion, (i) Wavelet and HIS based fusion, (j) Wavelet and PCA based fusion, (k) Casciola et al. with PCA Casciola et al. (2010), l) Wang et al. with PCA Wang, Shi, and Atkinson (2014b), (m) Lee et al. with PCA Lee and Yoon (2010), (n) Gaussian RBF with PCA, (o) Proposed interpolation method with HIS based fusion and (p) Proposed fusion method.

Table 1. Performance comparison of the interpolation methods after incorporating the PCA-based fusion technique for the first dataset.

	Quantative Parameter						
Interpolation Methods	ACC	RMSE	PSNR	ERGAS	UIQI	SSIM	Running Time (*Sec*)
Nearest Neighbour with HSI	0.8291	0.8867	20.2922	13.9293	0.5249	0.6070	3.732
Nearest Neighbour with PCA	0.8218	0.7106	24.9624	9.2740	0.6061	0.7385	4.683
Bi-linear with HSI	0.8426	0.4329	26.2695	10.6723	0.5627	0.6349	3.936
Bi-linear with PCA	0.8985	0.4150	28.9746	9.2754	0.6061	0.7384	4.867
Bi-cubic with HSI	0.8462	0.4421	28.2498	10.5448	0.5619	0.6406	5.044
Bi-cubic with PCA	0.9012	0.4023	34.9995	9.1218	0.6115	0.7489	5.995
Black Wavelet with HSI	0.8467	0.3984	32.1054	10.5848	0.7690	0.7438	5.632
Black Wavelet with PCA	0.9109	0.3017	34.9995	9.0014	0.7123	0.8202	6.583
Casciola et al. with PCA Casciola and Morigi (2010)	0.9252	0.2882	41.5800	8.7243	0.8595	0.9393	7.763
Wang et al. with PCA Wang, Shi, and Atkinson (2014b)	0.9371	0.2424	44.5023	7.2102	0.8932	0.9641	7.883
Lee et al. with PCA Lee and Yoon (2010)	0.9305	0.2508	43.8105	7.2364	0.8908	0.9705	7.821
Gaussian RBF with PCA	0.9126	0.3420	36.1834		0.8211	0.9000	7.012
Edge directed RBF with HSI	0.8954	0.2996	34.8700	8.3800	0.7829	0.8792	6.742
Proposed fusion method	0.9319	0.2406	44.7796	6.5001	0.8960	0.9669	7.983

figure. We can observe that the fused image generated by the proposed method is visually looking better compare to others. It preserves better luminous information. It can minimize artefacts like ringing or staircase curves across the edges in the PAN-sharpened image.

Extensive quantitative analysis by using the evaluation functions (Subsection 5.2) is also done to validate the proposed interpolation method. The performance of the standard, cutting-edge and the proposed interpolation methods are presented in Table 1.

We can observe that with respect to the Average Correlation Coefficient (ACC), Wang, Shi, and Atkinson (2014b) outperforms all other methods (including our proposed method). With respect to SSIM, the performance of Lee and Yoon (2010) is the best. However, regarding RMSE, PSNR, ERGAS, and UIQI, our proposed method outperformed all other methods. However, our method requires higher execution time (7.983 Seconds) compare to these techniques. We can also observe that the PCA-based algorithm for PAN-sharpening outperforms the HIS-based fusion technique in most of the cases.

In the second phase, we have collated the performance of the proposed algorithm with the Gaussian RBF, Edge-directed RBF and with the following eight cutting-edge PAN-sharpening algorithms:

(i) *GIHS* Te-Ming Tu et al. (2004): It is a spectral adjustment and HIS based fusion technique.
(ii) *GS* A and V (2000): It is a Gram-Schmidt transformation-based PAN-sharpening method.

(iii) *AWLP* Otazu et al. (2005): It is a wavelet-based fusion technique. In this method, some high-resolution PAN image's spatial information is fused into the low-resolution MS image, rather than injecting the complete PAN image.

(iv) *SVT* Zheng et al. (2008): It is a multi-scale Gaussian RBF-based interpolation and least-square support vector machine-based fusion method.

(v) *SRLD* Li, Yin, and Fang (2013): It is a dictionary learning and sparse portrayal-based PAN-sharpening technique.

(vi) *FI* Zhu and Bamler (2013): It is also a dictionary learning and sparse portrayal-based PAN-sharpening technique.

(vii) *VMFF* Shen et al. (2019b): It is a deep Convolutional Neural Network (CNN) and variation model-based fusion method. It uses the gradient information from the MS image to train the residual gradient CNN.

(viii) *CSSC* Zhang et al. (2019): It is a convolutional structure sparse coding-based method for PAN-sharpening.

We considered a radio-metrically corrected, geo-referenced dataset (acquired in November 2002) of Sundarban, India, obtained from the Quickbird satellite sensor to perform the experiment. It consists of a PAN image (Figure 6b) with 0.7 metre spatial resolution and an MS image (Figure 6a) with 2.8 metre spatial resolution. MS image contains the following four bands: i) Blue, ii) Green, iii) Red, iv) NIR. The reference VHR MS image (Figure 6c) with 0.7 metre spatial resolution is used to validate the PAN-sharpened image obtained by all methods. The proposed algorithm is executed on the images mentioned above. The value for λ is calculated as 4 ($\lambda = \frac{2.8}{0.7}$). The LR MS image is up-scaled by using the proposed interpolation technique. At that point, the HR PAN image is infused into the interpolated image to obtain the PAN-sharpened image.

After that, the reference and the interpolated images are used to compute ERGAS and UIQI by using Equation (8) and (9), respectively. Fused images generated by the proposed algorithm and these seven cutting-edge methods are presented in Figure 6d–m, respectively. We can see that the quality of the fused image obtained by the proposed algorithm is improved. In the fused image, artefacts across the edges are also minimized. The state-of-the-art methods' performances are also quantified by using the PAN-sharpened images generated by these algorithms and the reference image. Quantitative outcomes are summed up in Table 2.

We can observe that the proposed method performs better than these cutting-edge methods with the highest UIQI (0.957) and with the lowest ERGAS (1.629) with a running time of 7.810 Seconds. However, the method of Shen et al. Shen et al. (2019b) has shown better performance with respect to execution time compared to the proposed method.

6. Conclusion

In this study, we proposed a new methodology for edge-directed RBF-based multispectral image interpolation algorithm. The MS image is interpolated by a factor λ. We know that the interpolation factor should always be an integer value. Thus, for a fractional value for λ, re-sampling is applied to enlarge the image. Gaussian RBF is used to determine all in-determinant pixels from the enlarged image. We have shown that the second-order
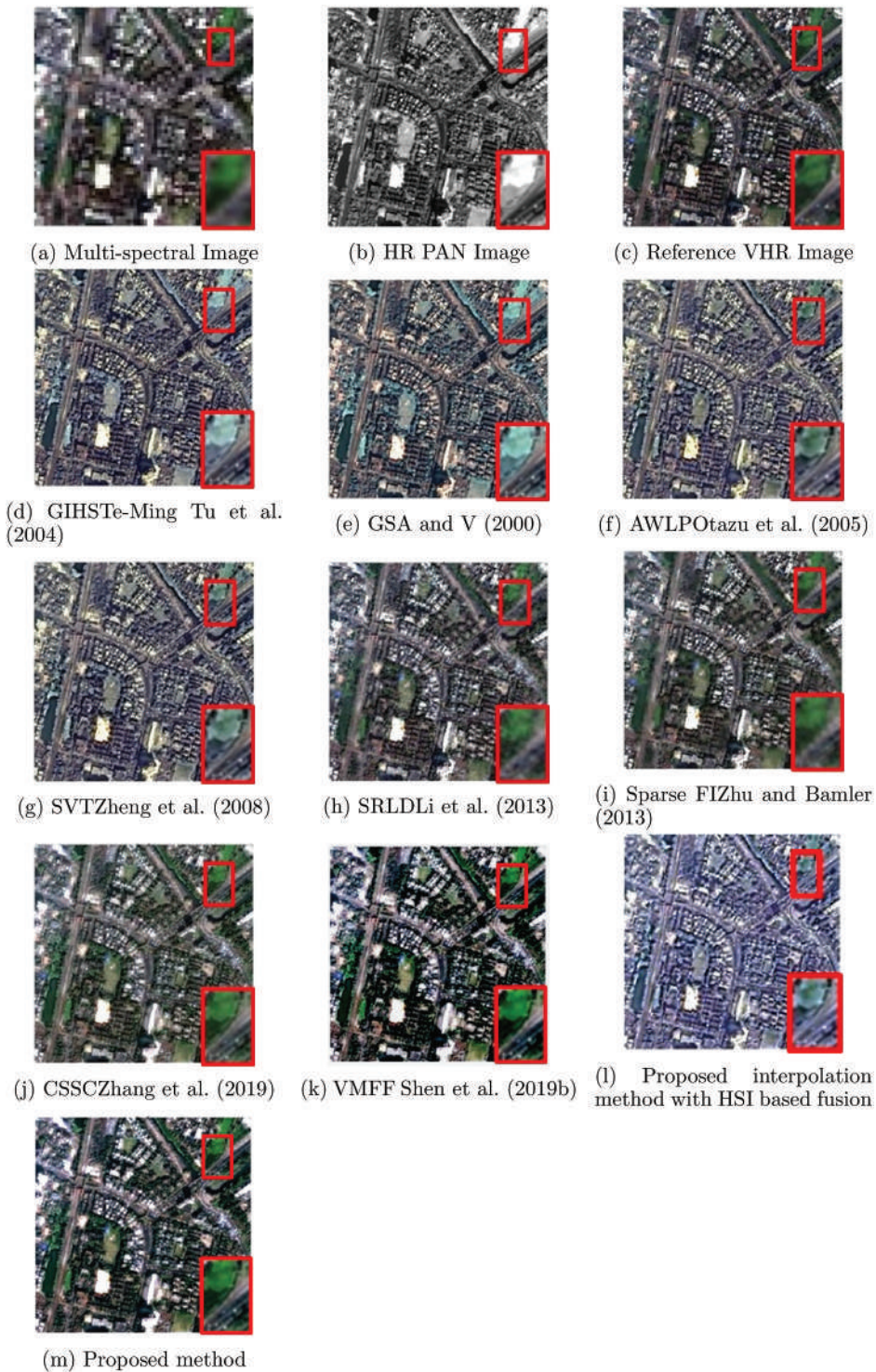
(a) Multi-spectral Image

(b) HR PAN Image

(c) Reference VHR Image

(d) GIHSTe-Ming Tu et al. (2004)

(e) GSA and V (2000)

(f) AWLPOtazu et al. (2005)

(g) SVTZheng et al. (2008)

(h) SRLDLi et al. (2013)

(i) Sparse FIZhu and Bamler (2013)

(j) CSSCZhang et al. (2019)

(k) VMFF Shen et al. (2019b)

(l) Proposed interpolation method with HSI based fusion

(m) Proposed method

Figure 6. Fusion results on the dataset of Sundarban, India, obtained from Quickbird: (a) LR MS image (spatial resolution = 2.8 metre), (b) HR-PAN image (spatial resolution =0.7 metre), c) Reference image (spatial resolution: 0.7 metre); fused image obtained by using: (d) GIHS Te-Ming Tu et al. (2004), (e) GS

A and V (2000), (f) AWLP Otazu et al. (2005), (g) Zheng et al. (2008), (h) SRLD Li, Yin, and Fang (2013), (i) Sparse FI Zhu and Bamler (2013), (j) CSSC Zhang et al. (2019),(k) VMFF Shen et al. (2019b) (l) Proposed interpolation method with HSI based fusion, and k) Proposed method for fusion.

Table 2. Quantitative result comparison with the cutting edge algorithms.

Method	UIQI	ERGAS	Running Time (*Sec*)
GIHS Te-Ming Tu et al. (2004)	0.776	3.383	11.215
GS A and V (2000)	0.777	3.196	10.818
AW LP Otazu et al. (2005)	0.924	1.967	12.305
SV T Zheng et al. (2008)	0.880	2.578	12.021
SRLD Li, Yin, and Fang (2013)	0.9287	2.001	15.920
Sparse F I Zhu and Bamler (2013)	0.938	1.884	16.000
V M F F Shen et al. (2019b)	0.952	1.891	7.550
CSSC Zhang et al. (2019)	0.940	2.042	11.664
Proposed interpolation method with HSI based fusion	0.883	2.220	6.160
Proposed method	0.957	1.629	7.810

derivative-based Laplacian of Gaussian (LoG) or Marr-Hildreth edge detection operator helps to preserve information and minimize the artefacts across the edges (in any direction) of the interpolated image. We have also considered the HR PAN image's edge information to increase the quality of the interpolated image. We have injected the HR-PAN image into the interpolated MS image by using the proposed PCA-based fusion algorithm. The proposed method's performance is quantified and validated with different standards and state-of-the-art techniques. We have considered one multi-source datasets obtained from CATROSAT-1 and LISS-IV. It outperforms all of them concerning most of the evaluation parameters. We have also compared the proposed algorithm with nine differ-ent cutting-edge methods by using another multi-sensor dataset obtained from Quickbird satellite sensor. The proposed method outperforms all cutting edge methods with respect to *UIQI* and *ERGAS*.

We know that the interpolation factor should always be an integer value. This limitation leads us to consider the re-sampling to fuse multi-source datasets with fractional interpolation factor. In some scenarios, it becomes a complex task where HR PAN image has a high spatial resolution (say less than 1 metre). During the re-sampling stage, up-sampling and down-sampling factors are large values (say $\lambda > 10$) to maintain the fractional factor. This approach suffers from the following shortcomings: i) loss of information, ii) generating spectral distortion, and iii) high space complexity. Finding out an alternative method to deal with the fractional interpolation factor is a thrust area of research. In the future, we will come up with a proper solution in this regard.

Disclosure statement

No potential conflict of interest was reported by the author(s).

ORCID

Somnath Mukhopadhyay ⓘ http://orcid.org/0000-0002-4532-6245

Data availability statement

The data that support the findings of this study are available on request from the co-author, Dr. Debasish Chakraborty (E-mail id: deba.isro@gmail.com).

References

Ablin, R., H. C. Sulochana, and G. Prabin. 2019. "An Investigation in Satellite Images Based on Image Enhancement Techniques." *European Journal of Remote Sensing 53*, 1–9.

Acharya, A., and S. Meher. 2012. "Region Adaptive Unsharp Masking Based Lanczos-3 Interpolation for Video Intra Frame Up-sampling." In *2012 Sixth International Con- Ference on Sensing Technology (ICST)*, Kolkata, India, 57–62.

Aiazzi, B., S. Baronti, F. Lotti, and M. Selva. 2009. "A Comparison between Global and Context-adaptive Pansharpening of Multispectral Images." *IEEE Geoscience and Remote Sensing Letters* 6 (2): 302–306. doi:10.1109/LGRS.2008.2012003.

Amro, I., J. Mateos, M. Vega, R. Molina, and A. Katsaggelos. 2011. "A Survey of Classical Methods and New Trends in Pansharpening of Multispectral Images." *EURASIP Journal on Advances in Signal Processing* 2011 (1): 79–101. doi:10.1186/1687-6180-2011-79.

Angelos, A., and A. Ioannis. 2009. "A Survey on Evaluation Methods for Image Inter- Polation." *Measurement Science and Technology* 20 (10): 104015. doi:10.1088/0957-0233/20/10/104015.

Arun, P. 2013. "A Comparative Analysis of Different Dem Interpolation Methods." *The Egyptian Journal of Remote Sensing and Space Science* 16 (2): 133–139. doi:10.1016/j.ejrs.2013.09.001.

Azam, S., F. T. Zohra, and M. M. Islam. 2014. "Remote Sensing Image Resolution Enlargement Algorithm Based on Wavelet Transformation." *International Journal of Image, Graphics and Signal Processing* 6 (6): 19. doi:10.5815/ijigsp.2014.06.03.

Baronti, S., B. Aiazzi, M. Selva, A. Garzelli, and L. Alparone. 2011. "A Theoretical Analysis of the Effects of Aliasing and Misregistration on Pansharpened Imagery." *IEEE Journal of Selected Topics in Signal Processing* 5 (3): 446–453. doi:10.1109/JSTSP.2011.2104938.

Bruzzone, L., L. Carlin, L. Alparone, S. Baronti, A. Garzelli, and F. Nencini. 2006. "Can Multiresolution Fusion Techniques Improve Classification Accuracy?" In *Image and Signal Processing for Remote Sensing XII*, edited by L. Bruzzone, 72–83. Vol. 6365. International Society for Optics and Photonics, Stockholm, Sweden.

Bureerat, S., and N. Pholdee. 2018. "Inverse Problem Based Differential Evolution for Efficient Structural Health Monitoring of Trusses." *Applied Soft Computing* 66: 462–472. doi:10.1016/j.asoc.2018.02.046.

Carper, W., T. Lillesand, and R. Kiefer. 1990. "The Use of Intensity-hue-saturation Transformations for Merging Spot Panchromatic and Multispectral Image Data." *Pho- Togramm. Eng. Remote Sens* 56 (3): 459467.

Casciola, G., L. Montefusco, and S. Morigi. 2010. "Edge-driven Image Interpolation Using Adaptive Anisotropic Radial Basis Functions." *Journal of Mathematical Imaging and Vision* 36 (2): 125–139. doi:10.1007/s10851-009-0176-8.

Casciola, G., S. Morigi, and S. Morigi. 2010. "Edge-driven Image Interpolation Using Adaptive Anisotropic Radial Basis Functions." *Journal of Mathematical Imaging and Vision* 36 (2): 125–139. doi:10.1007/s10851-009-0176-8.

Chavez, P., Jr., S. Sides, and J. Anderson. 1991. "Comparison of Three Different Methods to Merge Multiresolution and Multispectral Data: Landsat Tm and Spot Panchromatic." *Photogrammetric Engineering & Remote Sensing* 57 (3): 295–303.

Chavez, P. S., and A. Y. Kwarteng. 1989. "Extracting Spectral Contrast in Landsat Thematic Mapper Image Data Using Selective Principal Component Analysis." *Pho- Togrammetric Engineering and Remote Sensing* 55 (3): 339–348.

Chavez, P. S., Jr, S. C. Sides, and J. A. Anderson. 1990. "Comparison of Three Differ- Ent Methods to Merge Multiresolution and Multispectral Data: Landsat Tm and Spot Panchromatic." *AAPG Bulletin (American Association of Petroleum Geologists); (USA)* 74: 6.

Choi, M. 2006. "A New Intensity-hue-saturation Fusion Approach to Image Fusion with A Tradeoff Parameter." *IEEE Transactions on Geoscience and Remote Sensing* 44 (6): 1672–1682. doi:10.1109/TGRS.2006.869923.

Cunjun, L., L. Liangyun, W. Jihua, Z. Chunjiang, and W. Renchao. 2004. "Compar- Ison of Two Methods of the Fusion of Remote Sensing Images with Fidelity of Spectral Information".Vol. 4 *IGARSS 2004. 2004 IEEE International Geoscience and Remote Sensing Symposium*, Anchorage, AK, USA. 2561–2564.

Daamouche, A., and F. Melgani. 2009. "Swarm Intelligence Approach to Wavelet De- Sign for Hyperspectral Image Classification." *Geoscience and Remote Sensing Letters, IEEE* 6 (4): 825–829. doi:10.1109/LGRS.2009.2026191.

Dahiya, S., P. K. Garg, and M. K. Jat. 2013. "A Comparative Study of Various Pixel- Based Image Fusion Techniques as Applied to an Urban Environment." *International Journal of Image and Data Fusion* 4 (3): 197–213. doi:10.1080/19479832.2013.778335.

Demirel, H., and G. Anbarjafari. 2011. "Discrete Wavelet Transform-based Satellite Im Age Resolution Enhancement." *IEEE Transactions on Geoscience and Remote Sensing* 49 (6): 1997–2004. doi:10.1109/TGRS.2010.2100401.

Dennison, P. E., and D. A. Roberts. 2003. "Endmember Selection for Multiple End- Member Spectral Mixture Analysis Using Endmember Average Rmse." *Remote Sensing of Environment* 87 (2–3): 123–135. doi:10.1016/S0034-4257(03)00135-4.

Du, Q., N. Younan, R. King, and V. Shah. 2007. "On the Performance Evaluation of Pan-sharpening Techniques." *IEEE Geoscience Remote Sensing Letter* 4 (4): 518 522. doi:10.1109/LGRS.2007.896328.

Gao, L., X. Zhang, J. Gao, and S. You. 2019. "Fusion Image Based Radar Signal Feature Extraction and Modulation Recognition." *IEEE Access* 7: 13135–13148. doi:10.1109/ACCESS.2019.2892526.

Gowri, M., C. Kiruthika, S. Rengasamy, and T. Sharmila. 2015. "Satellite Image Fusion Based on Advanced Color Enhanced Ihs." IEEE Sponsored 2nd International Conference on Innovations in Information, Embedded and Communication Systems (ICIIECS) 2015, 10: 18675–18680.

Guo, X., Y. Tie, L. Ye, and J. Yan. 2018. "Identifying Facial Expression Using Adaptive Sub-layer Compensation Based Feature Extraction." *Journal of Visual Communication and Image Representation* 50: 65–73. doi:10.1016/j.jvcir.2017.11.007.

Han, W., J. Chu, L. Wang, and C. Pan. 2016. "Edge-directed Single Image Super- Resolution via Cross-resolution Sharpening Function Learning." *CCF Chinese Conference on Computer Vision 2015*, Xi'an, China.

Huang, W., and J. Liu. 2020. "Robust Seismic Image Interpolation with Mathematical Morphological Constraint." *IEEE Transactions on Image Processing* 29: 819–829. doi:10.1109/TIP.2019.2936744.

Hung, K.-W., and W.-C. Siui. 2012. "Robust Soft-decision Interpolation Using Weighted Least Squares." *IEEE Transactions on Image Processing* 21 (3): 1061–1069. doi:10.1109/TIP.2011.2168416.

Huynh-Thu, Q., and M. Ghanbari. 2008. "Scope of Validity of Psnr in Image/video Quality Assessment." *Electronics Letters* 44 (1): 800–801. doi:10.1049/el:20080522.

Hwang, J. W., and H. S. Lee. 2004. "Adaptive Image Interpolation Based on Local Gradient Features." *IEEE Signal Processing Letters* 11 (3): 359–362. doi:10.1109/LSP.2003.821718.

Ji, J., B. Zhong, and -K.-K. Ma. 2020. "Image Interpolation Using Multi-scale Attention-aware Inception Network." *IEEE Transactions on Image Processing* 29: 9413–9428. doi:10.1109/TIP.2020.3026632.

Karimi, E., K. Kangarloo, and S. Javadi. 2014. "A Survey on Super-resolution Meth- Ods for Image Reconstruction." *International Journal of Computer Applications* 90 (3): 32–39. doi:10.5120/15557-4300.

Kaur, I., and N. Neeru. 2017. "A Theoretical Analysis Towards Remote Sensing Using Image Fusion: A Review." *International Journal of Advanced Research in Computer Science* 8: 7.

Kim, T., J. Kim, and J. Park. 2020. "Image Re-sampling from a Perspective of Wave Field Propagation." In *2020 International Conference on Information and Commu- Nication Technology Convergence (ICTC)*, 1423–1425. Jeju, Korea (South).

Lee, Y. J., and J. Yoon. 2010. "Nonlinear Image Upsampling Method Based on Radial Basis Function Interpolation." *IEEE Transactions on Image Processing* 19 (10): 2682–2692. doi:10.1109/TIP.2010.2050108.

Li, H., L. Jing, Y. Tang, and L. Wang. 2018. "An Image Fusion Method Based on Image Segmentation for High-resolution Remotely-sensed Imagery." *Remote Sensing* 10 (5): 790. doi:10.3390/rs10050790.

Li, S., H. Yin, and L. Fang. 2013. "Remote Sensing Image Fusion via Sparse Repre- Sentations over Learned Dictionaries." *IEEE Transactions on Geoscience and Remote Sensing* 51 (9): 4779–4789. doi:10.1109/TGRS.2012.2230332.

Li, X., and M. Orchard. 2001. "New Edge-directed Interpolation." *IEEE Transactions on Image Processing* 10 (10): 1521–1527. doi:10.1109/83.951537.

Madhukar, B. N., and R. Narendra. 2013. "Lanczos Resampling for the Digital Process-ing of Remotely Sensed Images." In *Proceedings of International Conference on VLSI, Communication, Advanced Devices, Signals & Systems and Networking (VCASAN- 2013)*, 403–411. India: Springer India.

Meng, X., H. Shen, H. Li, L. Zhang, and R. Fu. 2019. "Review of the Pansharpening Methods for Remote Sensing Images Based on the Idea of Meta-analysis: Practical Discussion and Challenges." *Information Fusion* 46: 102–113. doi:10.1016/j.inffus.2018.05.006.

Moraes, T., P. Amorim, J. V. D. Silva, and H. Pedrini. 2020. "Medical Image Interpolation Based on 3d Lanczos Filtering." *Computer Methods in Biomechanics and Biomedical Engineering: Imaging & Visualization* 8 (3): 294–300.

Mukhopadhyay, S., M. Paul, R. Pal, and D. De. 2020. "Tea Leaf Disease Detection Using Multi-objective Image Segmentation." *Multimedia Tools and Applications* 80: 1573–7721.

Muzhou, H., and H. Xuli. 2011. "The Multidimensional Function Approximation Based on Constructive Wavelet Rbf Neural Network." *Applied Soft Computing* 11 (2): 2173–2177. doi:10.1016/j.asoc.2010.07.016.

Ooi, S. Y., A. B. J. Teoh, Y. H. Pang, and B. Y. Hiew. 2016. "Image-based Hand- Written Signature Verification Using Hybrid Methods of Discrete Radon Transform, Principal Component Analysis and Probabilistic Neural Network." *Applied Soft Computing* 40: 274–282. doi:10.1016/j.asoc.2015.11.039.

Otazu, X., M. Gonzalez-Audicana, O. Fors, and J. Nunez. 2005. "Introduction of Sensor Spectral Response into Image Fusion Methods. Application to Wavelet-based Methods." *IEEE Transactions on Geoscience and Remote Sensing* 43 (10): 2376–2385. doi:10.1109/TGRS.2005.856106.

Ozelkan, E., S. Bagis, E. C. Ozelkan, B. B. Ustundag, M. Yucel, and C. Ormeci. 2015. "Spatial Interpolation of Climatic Variables Using Land Surface Temperature and Modified Inverse Distance Weighting." *International Journal of Remote Sensing* 36 (4): 1000–1025. doi:10.1080/01431161.2015.1007248.

Panchal, S., and R. Thakker. 2015. "Implementation and Comparative Quantitative Assessment of Different Multispectral Image Pansharpening Approches." *arXiv Preprint arXiv:1511.04659*.

Pflugfelder, D., and H. Scharr. 2020. "Practically Lossless Affine Image Transformation." *IEEE Transactions on Image Processing* 29: 5367–5373. doi:10.1109/TIP.2020.2982260.

Pohl, C., and J. van Genderen. 1998. "Multisensor Image Fusion in Remote Sensing: Concepts, Methods and Applications." *International Journal of Remote Sensing* 19 (5): 823–854. doi:10.1080/014311698215748.

Shahdoosti, H. R., and H. Ghassemian. 2016. "Combining the Spectral Pca and Spatial Pca Fusion Methods by an Optimal Filter." *Information Fusion* 27: 150–160. doi:10.1016/j.inffus.2015.06.006.

Shen, H., M. Jiang, J. Li, Q. Yuan, Y. Wei, and L. Zhang. 2019a. "Spatial-spectral Fusion by Combining Deep Learning and Variational Model." *IEEE Transactions on Geoscience and Remote Sensing* 57 (8): 6169–6181. doi:10.1109/TGRS.2019.2904659.

Shen, H., M. Jiang, J. Li, Q. Yuan, Y. Wei, and L. Zhang. 2019b. "Spatial spectral Fusion by Combining Deep Learning and Variational Model." *IEEE Transactions on Geoscience and Remote Sensing* 57 (8): 6169–6181. doi:10.1109/TGRS.2019.2904659.

Shreyas, F. 2014. "Image Interpolation Techniques in Digital Image Processing: An Overview." *International Journal of Engineering Research and Application* 4: 70–73.

Singh, G., and G. Goyal (2015). Linear Image Upscaling: Areveiw.

Te-Ming, T., P. S. Huang, C.-L. Hung, and C.-P. Chang. 2004. "A Fast Intensity-hue-saturation Fusion Technique with Spectral Adjustment for Ikonos Im- Agery." *IEEE Geoscience and Remote Sensing Letters* 1 (4): 309–312. doi:10.1109/LGRS.2004.834804.

Temizel, A. (2007). Image Resolution Enhancement Using Wavelet Domain Hidden Markov Tree and Coefficient Sign Estimation. In *2007 IEEE International Conference on Image Processing*, Vol. 5, V–381. San Antonio, TX, USA: IEEE.

Teoh, K. K., H. Ibrahim, and S. K. Bejo (2008). Investigation on Several Basic Interpo- Lation Methods for the Use in Remote Sensing Application. In *2008 IEEE Conference on Innovative Technologies in Intelligent Systems and Industrial Applications*, Cyberjaya, Malaysia. 60–65.

Venkatakrishnamoorthy, T., and G. U. Reddy. 2019. "Cloud Enhancement of NOAA Multispectral Images by Using Independent Component Analysis and Principal Component Analysis for Sustainable Systems." *Computers & Electrical Engineering* 74: 35–46. doi:10.1016/j.compeleceng.2019.01.005.

Wang, Q., W. Shi, and P. Atkinson. 2014a. "Sub-pixel Mapping of Remote Sensing Images Based on Radial Basis Function Interpolation." *ISPRS Journal of Photogram- Metry and Remote Sensing* 92: 115.

Wang, Q., W. Shi, and P. M. Atkinson. 2014b. "Sub-pixel Mapping of Remote Sensing Images Based on Radial Basis Function Interpolation." *ISPRS Journal of Photogram- Metry and Remote Sensing* 92: 1–15. doi:10.1016/j.isprsjprs.2014.02.012.

Wang, Z., and A. Bovik. 2002. "A Universal Image Quality Index." *IEEE Signal Pro- Cessing Letters* 9 (3): 81–84. doi:10.1109/97.995823.

Wang, Z., A. Bovik, H. Sheikh, and E. Simoncelli. 2004. "Image Quality Assessment: From Error Visibility to Structural Similarity." *IEEE Transactions on Image Processing* 13 (4): 600–612. doi:10.1109/TIP.2003.819861.

Wang, Z., D. Ziou, C. Armenakis, D. Li, and Q. Li. 2005. "A Comparative Analysis of Image Fusion Methods." *Geoscience and Remote Sensing, IEEE Transactions On* 43: 1391–1402.

Zhang, K., F. Zhang, and S. Yang. 2019. "Fusion of Multispectral and Panchromatic Images via Spatial Weighted Neighbor Embedding." *Remote Sensing* 11 (5): 557. doi:10.3390/rs11050557.

Zhang, K., M. Wang, S. Yang, and L. Jiao. 2019. "Convolution Structure Sparse Coding for Fusion of Panchromatic and Multispectral Images." *IEEE Transactions on Geoscience and Remote Sensing* 57 (2): 1117–1130. doi:10.1109/TGRS.2018.2864750.

Zhang, X., Wu, and X. Xiaolin. 2008. "Image Interpolation by Adaptive 2-d Autoregressive Modeling and Soft-decision Estimation." *IEEE Transactions on Image Processing* 17 (6): 887–896. doi:10.1109/TIP.2008.924279.

Zheng, S., W. Shi, J. Liu, and J. Tian. 2008. "Remote Sensing Image Fusion Using Multiscale Mapped Ls-svm." *IEEE Transactions on Geoscience and Remote Sensing* 46 (5): 1313–1322. doi:10.1109/TGRS.2007.912737.

Zhou, X., J. Liu, S. Liu, L. Cao, Q. Zhou, and H. Huang. 2014. "A Gihs-based Spectral Preservation Fusion Method for Remote Sensing Images Using Edge Restored Spectral Modulation." *ISPRS Journal of Photogrammetry and Remote Sensing* 88: 16–27. doi:10.1016/j.isprsjprs.2013.11.011.

Zhu, X. X., and R. Bamler. 2013. "A Sparse Image Fusion Algorithm with Applica- Tion to Pan-sharpening." *IEEE Transactions on Geoscience and Remote Sensing* 51 (5): 2827–2836. doi:10.1109/TGRS.2012.2213604.